Supplementary information

Supplementary materials for

Growing human-induced climate change footprint in regional weekly fire extremes

Sifang Feng[1,2,*]; Jakob Zscheischler[2,3]; Zengchao Hao[1]; Emanuele Bevacqua[2,*]

[1] College of Water Sciences, Beijing Normal University, Beijing, China

[2] Department of Compound Environmental Risks, Helmholtz Centre for Environmental Research – UFZ, Leipzig, Germany

[3] Department of Hydro Sciences, TUD Dresden University of Technology, Dresden, Germany

[*] Corresponding author: Sifang Feng (fengsf@mail.bnu.edu.cn); Emanuele Bevacqua (emanuele.bevacqua@ufz.de)

Comparison of performance between grid model and regional model

To inspect whether FWI predicts weekly fires better when focussing on regional or grid scales, we also applied a logistic regression considering both grid values of FWI and burned area (hereinafter *grid-cell model*, see Supplemental Methods). Then, we applied the Log-Loss skill score to evaluate the model performance and compared such skill scores between grid-cell model and regional model. The grid-cell model shows a low performance (0.08, spatially weighted average of the Log-Loss skill scores), which is consistent with a generally low Spearman FWI-BA correlation over most grid cells (Figure S11a and Figure S12a). In contrast, at IPCC regions, the FWI-BA correlations are larger; specifically, they typically surpass the regional median of grid-scale correlations over most regions and even exceed the 99th percentile of grid-scale correlations over some regions (Figure S11b-c). Accordingly, across most regions, the regional model performance (0.11, average of the regional Log-Loss skill scores) is better than the grid-cell model (0.08) (Figure 1a and Figure S12a-b). Such better performance of the regional model is also confirmed by a comparison of the skill score's cumulative distribution function (CDF) for the grid-cell and regional models (Figure S12c). Similar improvements are observed with other performance metrics, such as the skill score of Brier score and PR-AUC (Figure S12d,e). The higher performance in the regional model may arise from the regional aggregation that may smooth the influence of localized factors on fire in the grid model (for instance, topography and socioeconomic drivers) which may obscure a potential clear FWI-BA relationship[54]. Therefore, we considered regional fires for further analysis due to the higher predictive confidence of FWI for weekly fire extremes at this scale.

Supplemental Methods

To assess whether the weather-fire relationship based on the logistic regression model really works better for regionally aggregated BA than BA at individual grid cells, in each grid cell, we also applied the same 80%-based methodology with the regional fire season to define the gridded fire season (Figure S13).

We then defined extreme fire events occurrence at each grid cell during the fire season of 2002-2015 based on the same 85th-based approach with the regional fire. To better fit the upcoming model for building the FWI-BA relationship, we only focused on grids where the threshold is above zero (Figure S10c). The fraction of BA caused by pre-defined extreme fire to the total burned area during the fire season for 2002-2015 shown in Figure S10d. Spatially-weighted averaging across grid cells, we found that extreme fires accounted for about 87% of the total burned area at the grid cells and the fraction is equal to 100% over many grid cells. Then, we applied a logistic regression model to estimate the probability of extreme fire as a function of FWI over selected grid (hereinafter *grid-cell model*) with the equation 1 and evaluated performance of grid-cell model using the same scoring methods with regional model: the Log-Loss score (Log-Loss), the Brier Score (BS), and an area under the Precision-Recall curve (PR-AUC).

To identify an appropriate spatial scale for the weather-fire relationship, we computed spatially weighted average skill scores across grid cells where we fitted the grid-cell model and the average of skill scores over IPCC regions where we fitted the regional model (that is, where the threshold of 85th percentile is above zero). In addition, we also compared the cumulative distribution function (CDF) of the skill score across grid cells from the grid-cell and across regions from the regional model. Finally, we selected the spatial scale with a higher model performance by comparing such average skill scores and CDF at the two spatial scales.

Supplemental Figures and tables

Table S1. Summary of existing fire attribution studies. Here, the detection method indicates the approach to detecting human-induced climate change.

Reference	Weather variables	Fire metric	Weather-fire relationship	Detection method	Human-induced climate change	Study area
This study	FWI (T, P, RH, and Wind)	Extreme fire (weekly burned area higher than 85th percentile)	Logistic regression model	Scaling factor	From FWI, T, P, RH, and Wind	IPCC regions
16	T, VPD, P and Wind	Extreme fire (daily burned area above 10,000 acres)	Machine learning model	Comparison historical temperature with preindustrial temperature from climate models	From T	California
20	Tmax	Monthly burned area	Linear regression model	Comparison Hist ensemble with Nat ensemble from climate models	From T	California
22	P	monthly burned area, fire emissions of CO2 and PM2.5	Linear regression model	Comparison Hist ensemble with Nat ensemble from the MIROC5 model	From P	equatorial Asia
21	FM1000 and FFWI	Large wildfire (the largest 15% of daily fall burned area)	Logistic regression model	50-year low-pass filtered simulation from climate models	From T and RH	California
17	Fuel aridity metrics (ETo, VPD, CWD, PDSI, FWI, ERC, FFDI, and KBDI)	Annual burned area	Linear regression model	50-year low-pass filtered simulation from climate models	From T and VPD	western United States
19	T	five year total area burned	Linear regression model	Optimal detection approach based on simulated area-burned-weighted T from CGCM2	From T	Canada

The full names of the abbreviations in the table describe: FWI, Fire Weather Index; T, temperature; P, precipitation; RH: relative humidity; Wind, Wind speed; VPD, Vapor Pressure Deficit; Nat ensemble, simulations under natural-only forcing from climate models; Hist ensemble, simulation under historical (natural+anthropogenic) forcing from climate models; FM1000, 1000-hour dead fuel moisture; FFWI: Fosberg Fire Weather Index; ETo, reference potential evapotranspiration; CWD, climatic water deficit; PDSI, Palmer drought severity index; ERC, Energy Release Component; FFDI, McArthur forest fire danger index; KBDI, Keetch–Byram drought index; CGCM2, second Canadian Climate Centre for Modelling and Analysis model;

Table S2. **List of selected CMIP6 climate models.**

Models	Ensembles	Spatial resolution (Lat × Lon)
ACCESS-CM2	r1i1p1f1	144 × 192
ACCESS-ESM1-5	r1i1p1f1	145 × 192
CMCC-ESM2	r1i1p1f1	192 × 288
CanESM5	r1i1p1f1	64 × 128
EC-Earth3	r1i1p1f1	256 × 512
FGOALS-g3	r1i1p1f1	80 × 180
INM-CM4-8	r1i1p1f1	120 × 180
INM-CM5-0	r1i1p1f1	120 × 180
IPSL-CM6A-LR	r1i1p1f1	143 × 144
MIROC-ES2L	r1i1p1f2	64 × 128
MIROC6	r1i1p1f1	128 × 256
MPI-ESM1-2-HR	r1i1p1f1	192 × 384
MPI-ESM1-2-LR	r1i1p1f1	96 × 192
MRI-ESM2-0	r1i1p1f1	160 × 320

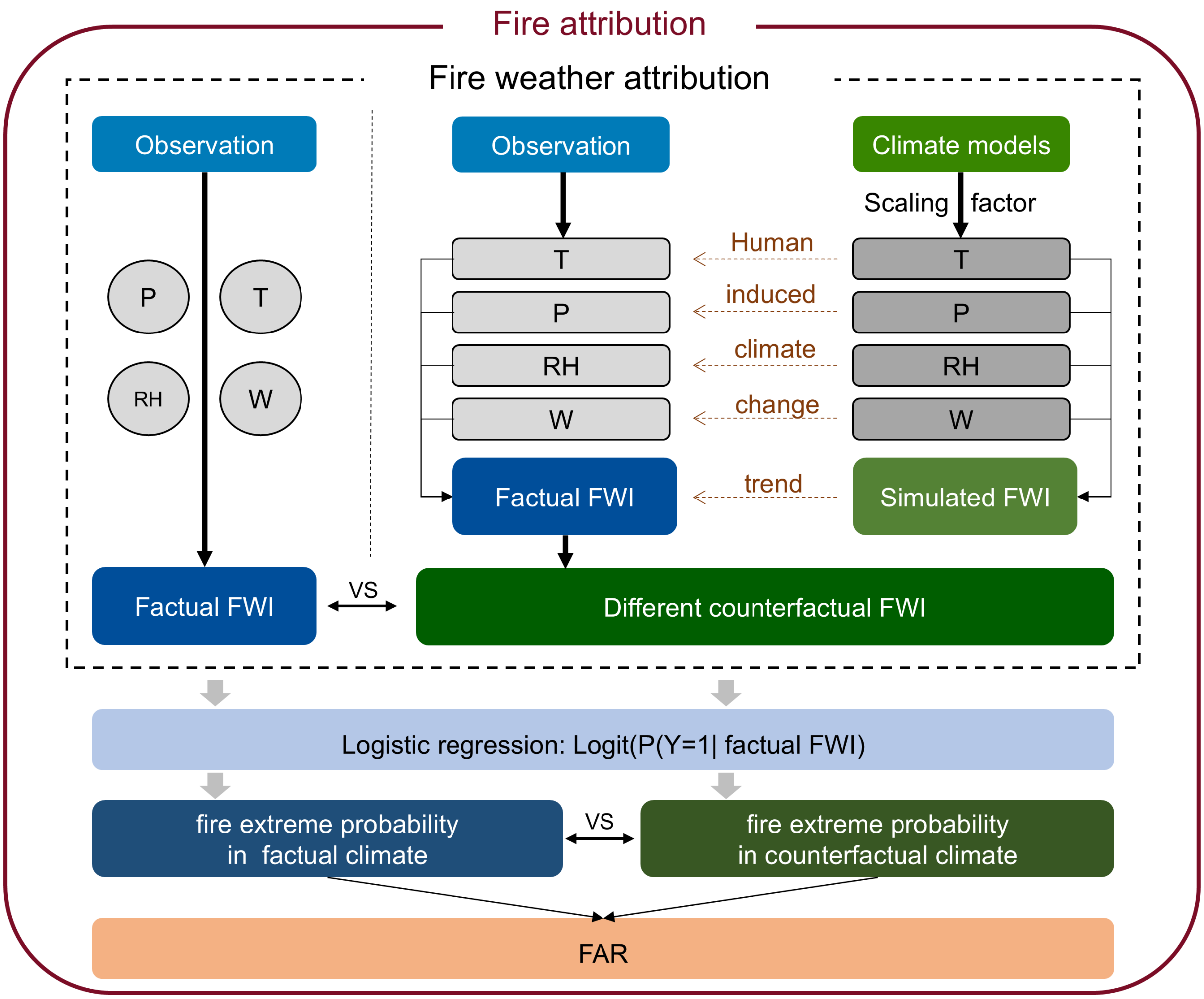

Figure S1. **Schematic of the approach employed for attributing fires to human-induced climate change.** The factual Fire Weather Index (FWI) is derived from observed precipitation (P), temperature (T), relative humidity (RH), and wind speed (W). We selected the logistic regression model linking factual FWI to observed fire extremes (Y) to predict the probability of extreme fire occurrence in factual climates. Extreme fires are defined based on the 85th percentile of burned areas time series. Then, we applied scaling factors from climate models to remove the human-induced climate change from factual FWI, obtaining counterfactual FWI. The pre-defined logistic regression fitted to the factual FWI is applied to counterfactual FWI to predict the probability of extreme fire occurrence in counterfactual climates. Finally, fire attribution is achieved by applying the fraction of attributable risk (FAR) to compare the predicted probability of extreme fire in factual and counterfactual climates. In addition, we applied the same approach above but for different counterfactual FWIs by removing human-induced climate change in individual FWI drivers on fire extremes to quantify the contribution of human-induced climate change in individual drivers on fire extremes.

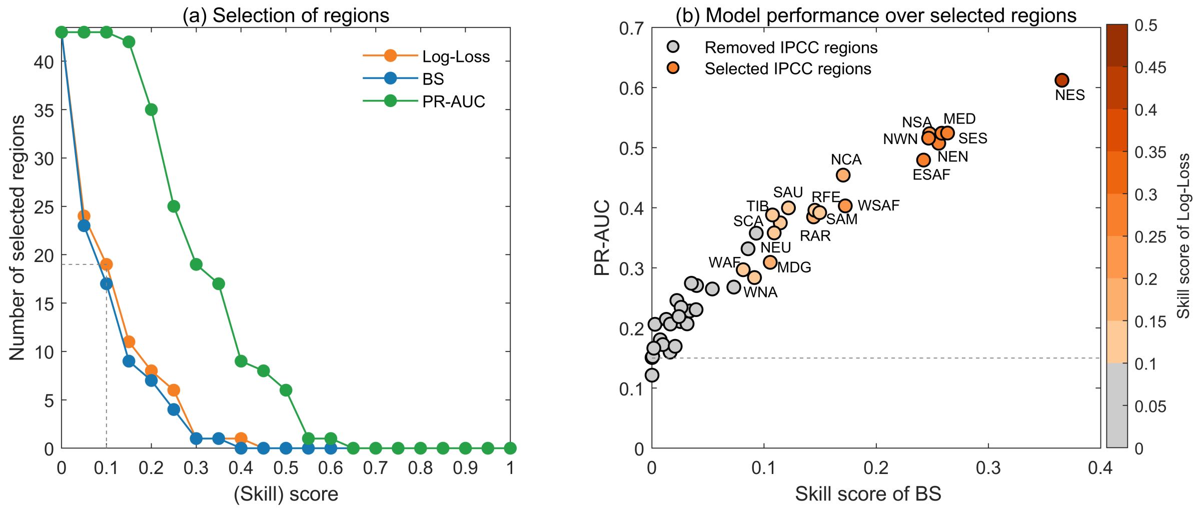

Figure S2. **Rules for selecting regions with good model's skill.** (a) The number of selected regions conditional to different (skill) scores of Log-Loss (yellow line), Brier score (BS, blue line), and an area under the Precision-Recall curve (PR-AUC, green line). 19 IPCC regions are selected with higher Log-Loss skill scores than the baseline we set (0.1). (b) Scatter plot between skill score of BS (x-axis) and PR-AUC (y-axis) over each region. A grey (yellow) circle indicates an IPCC region that is not selected (selected) with the color representing the skill score of Log-Loss. The text next to the yellow circles shows the abbreviations for the names of the selected IPCC regions.

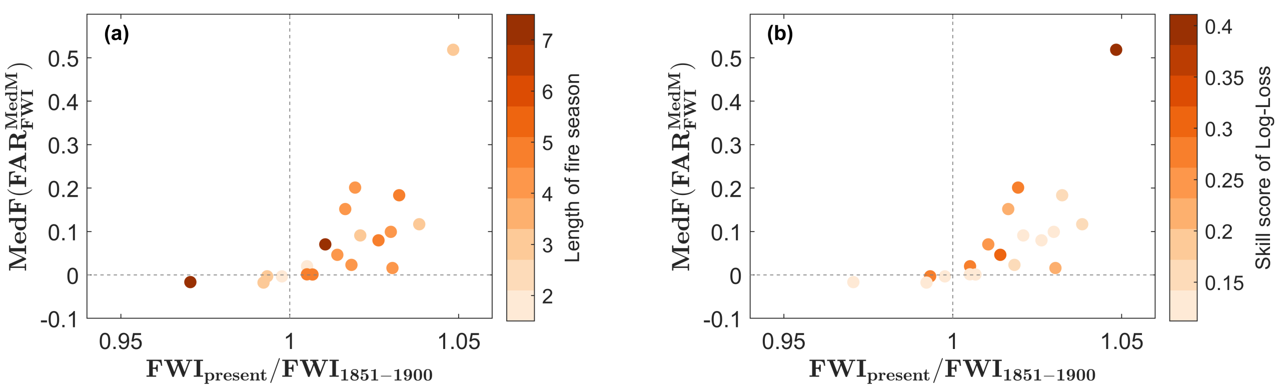

Figure S3. **The role of the length of fire season and performance of logistic regression model in shaping the human-induced climate change effect on regional fire extreme.** Scatter plot showing the relationship between the human-induced climate change influence on extreme fire ($MedF(FAR_{FWI}^{MedM})$ from Figure 2b, y-axes) and human-induced climate change in FWI ($FWI_{present}/FWI_{1900}$ from Figure 2a, x-axes) during 2002-2015 fire season. Each circle in panels a and b indicates each selected region with color representing the length of fire season (a) and skill score of log loss (b), respectively.

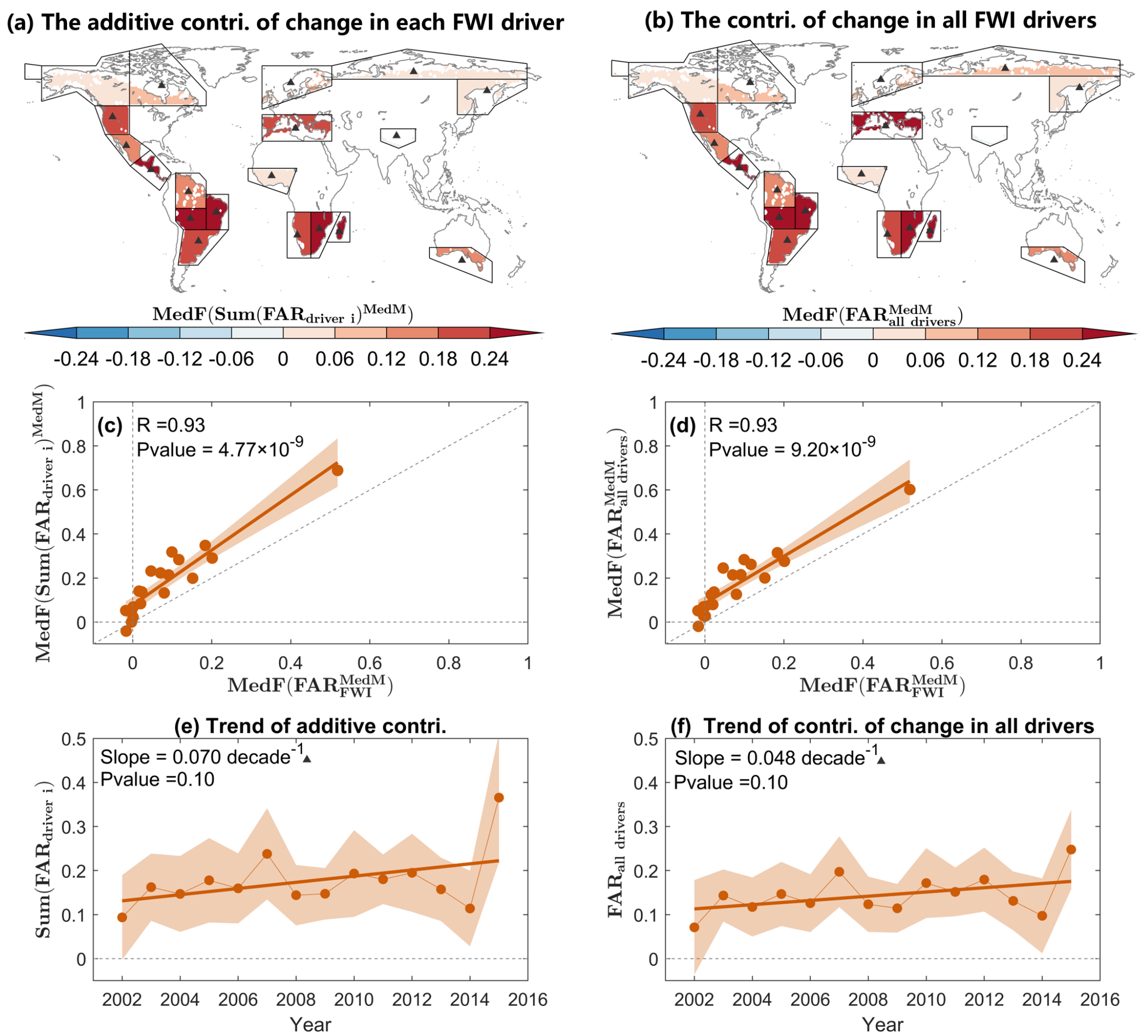

Figure S4. The contribution of human-induced climate change from all Fire Weather Index (FWI) meteorological drivers on fire extremes during 2002-2015 fire season. (a) Similar to Figure 2b, but for the sum of four separate the fraction of attributable risk (FAR) ($MedF(Sum(FAR_{driver\,i})^{MedM})$) based on counterfactual FWI where the change in individual drivers– that is, temperature (i = T), precipitation (i = P), relative humidity (i = RH), and wind speed (i = W)– are removed once at a time, respectively (see Methods) over selected regions. (b) Similar to Figure 2b, but for the FAR based on counterfactual FWI where the change in all drivers are removed at a time ($MedF(FAR^{MedM}_{all\,drivers})$, see Methods). The black triangles in panel a-b indicate that more than 70% of extreme fire events agree on the sign of the change. (c) Scatter plot showing the relationship between $MedF(FAR^{MedM}_{FWI})$ from Figure 2b and $MedF(Sum(FAR_{driver\,i})^{MedM})$ from panel a with orange points indicating regional values over selected IPCC region. The numbers in the upper left indicate the Pearson correlation coefficient between them and their P-value. The linear regression line is shown with shading indicating its two-sided 95% confidence interval. (d) Similar to panel c but for relationship between $MedF(FAR^{MedM}_{FWI})$ and $MedF(FAR^{MedM}_{all\,drivers})$ from panel b. (e-f) Similar to Figure 5b but for annual impact of the sum of four separate FARs from individual drivers ($Sum(FAR_{driver\,i})$, panel e) and the FAR from counterfactual FWI where change in all drivers are removed at a time ($FAR_{all\,drivers}$, panel f) on the probability of extreme fire events (see Methods).

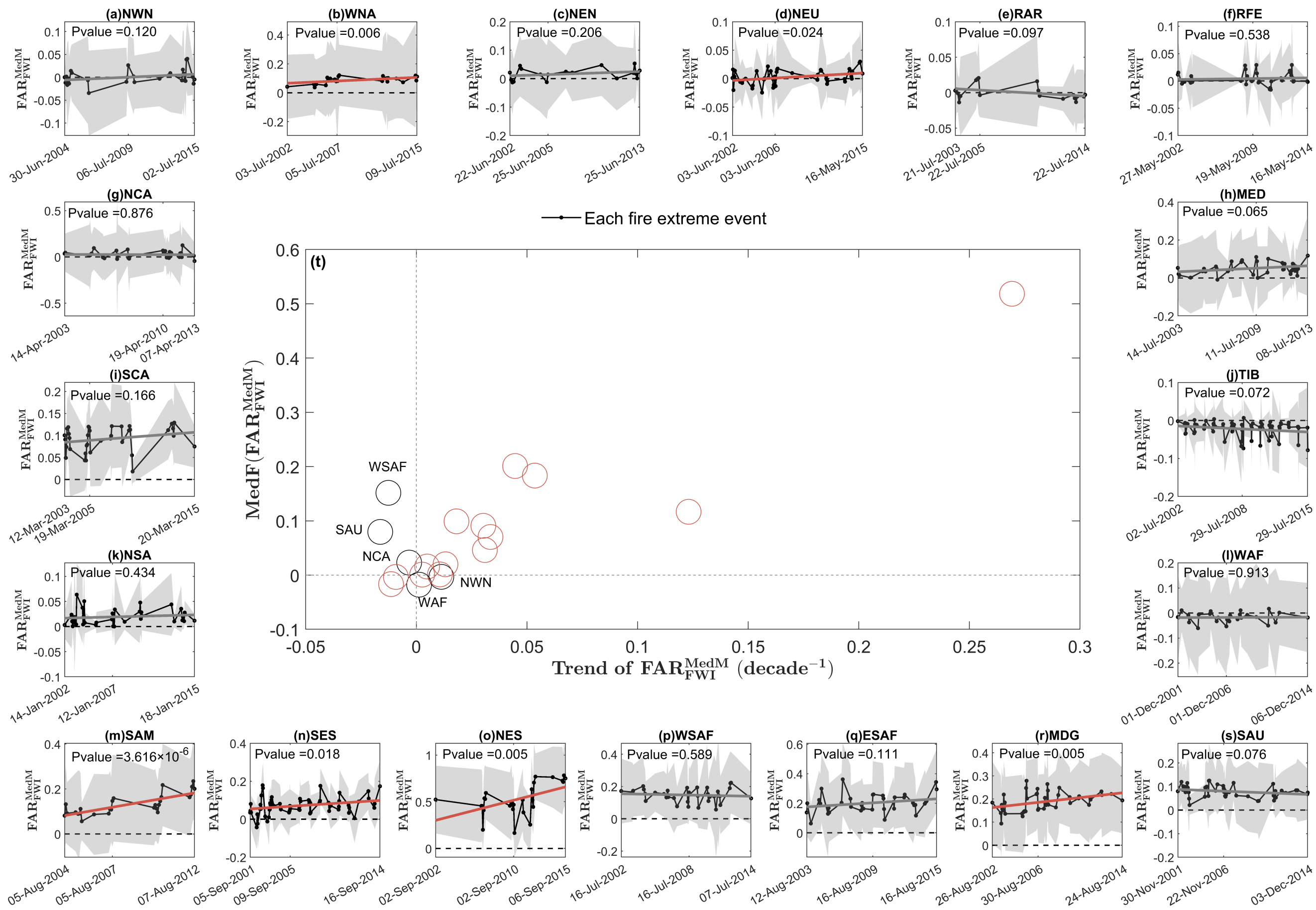

Figure S5. **The trends of the human-induced climate change influence on each regional extreme fire over weekly fire extreme occurrence date during 2002-2015 fire season.** (a-s) For individual regions, the linear trend (black line with dots) in the multimodel median of human-induced climate change of Fire Weather Index (FWI) influence on the predicted probability of each extreme fire event (FAR_{FWI}^{MedM}, y-axes) across fire dates (see Methods) – The trend is illustrated by the linear regression line with its P-value. The shading indicates that ± 1 standard deviation of multiple climate models for each fire. Red lines indicate the regression lines with the significant positive trend at the 0.05 significant level while grey lines indicate the insignificant trend. (t) The scatter plot between the slope of the regression line from panel a-s (trend of FAR_{FWI}^{MedM}, x-axis) and the human-induced climate change influence on fire extremes ($MedF(FAR_{FWI}^{MedM})$, y-axis) from Figure 2b over each region. Red (grey) circles indicate regions where $MedF(FAR_{FWI}^{MedM})$ and the trend of FAR_{FWI}^{MedM} have the same (different) symbols.

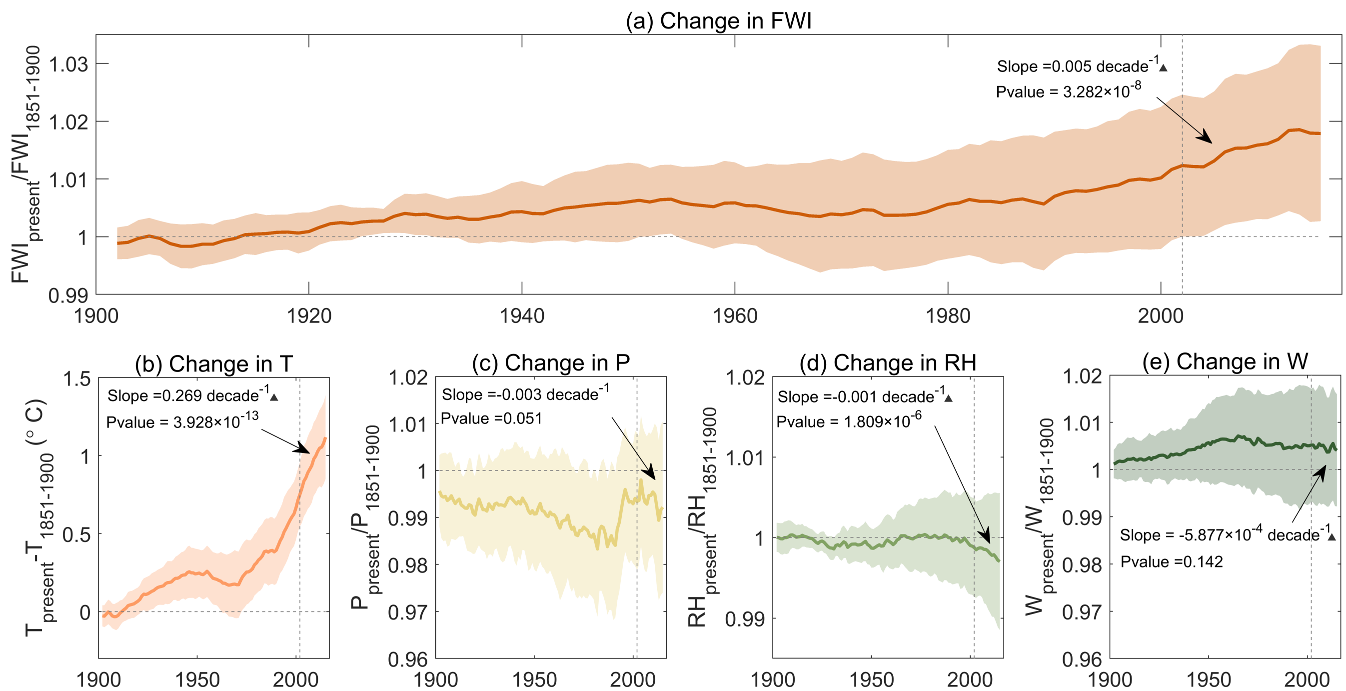

Figure S6. The trends of change in FWI and its meteorological drivers during fire season of 1901-2015. (a) The annual trends of change in FWI from 1901 to 2015 ($FWI_{present}/FWI_{1851-1900}$) defined as the ratio of conditions in 1901-2015 to preindustrial conditions in 1851-1900 based on a 15-year window centered on the considered year (x-axis). The yearly ratio is obtained by first computing median $FWI_{present}/FWI_{1851-1900}$ across all months of fire season of all regions for each year given one climate model and then computing multimodel median (regional values are derived based on the median of ratio across grid cells of each region). The shading indicates ± one standard deviation of multiple climate models. The numbers indicate the slope of the regression line for multimodel median change in FWI (solid line) from 2002 to 2015 and its P-value. The black triangle indicates that over 70% of climate models agree on the sign of trend. (b) Similar to panel a but for annual trends of change in temperature (b, $T_{present} - T_{1851-1900}$), defined as the difference between conditions in 1901-2015 and preindustrial conditions in 1851-1900. (c-e) Similar to panel a but for annual trends of change in precipitation (C, $P_{present}/P_{1851-1900}$), change in relative humidity (d, $RH_{present}/RH_{1851-1900}$), and change in wind speed (e, $W_{present}/W_{1851-1900}$).

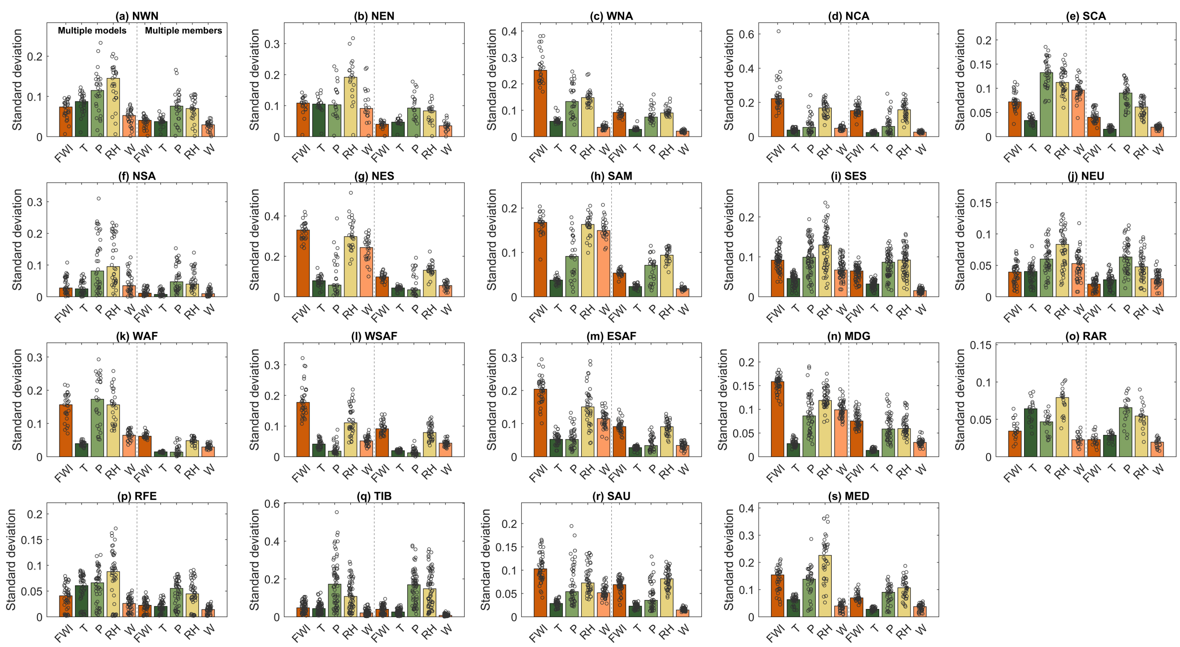

Figure S7. Uncertainty due to climate models and internal natural variability in the human-induced climate change effect on each extreme fire over selected regions during the fire season of 2002-2015. (a-s) For each region, the first bar to the left of the dashed line indicates uncertainty due to climate models in the effect of human-induced climate change in FWI, obtained by first computing one standard deviation of the fraction of attributable risk (FAR) across 14 climate models given one extreme fire events and then computing the median of such standard deviations across all events (see Methods). Black points indicate one standard deviation of FARs across multiple models for each fire event. The other four bars to the left of the dashed line are similar to the first one but for FAR based on four counterfactual FWIs where the changes in temperature (T), precipitation (P), relative humidity (RH), and wind speed (W) were removed once at a time. The five bars to the right of the dashed line are similar to those on the left side but indicate the uncertainty due to internal natural variability, based on fifty ensemble members of the climate model CanESM2.

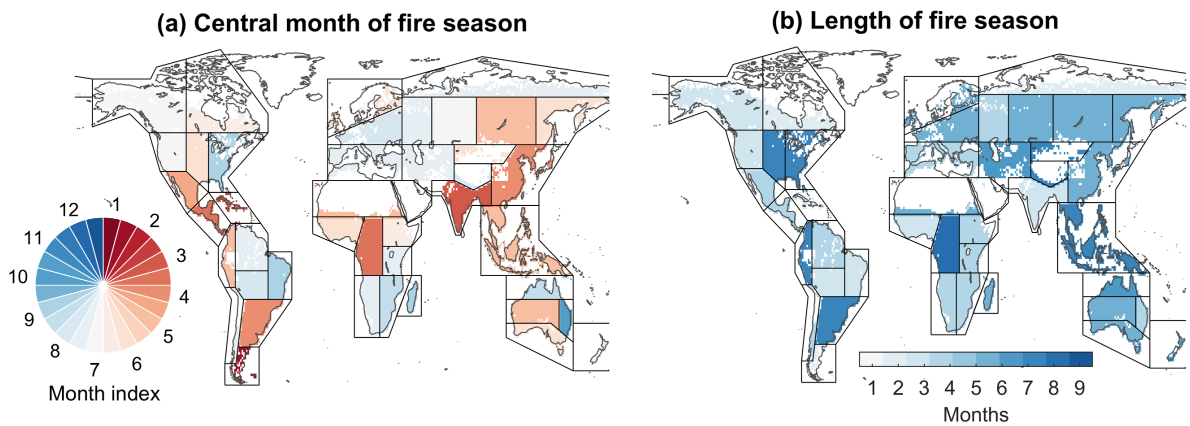

Figure S8. The regional fire season over each IPCC region. (a) Central month of fire season and (b) fire season length at each region. The fire season over each region is defined as the fewest consecutive months, accounting for at least 80% of the annual burned area (see Methods). The circular legend in the lower left of the panel a uses a 0.5 interval scale from 1 to 12.5 to consider the non-integer central months index.

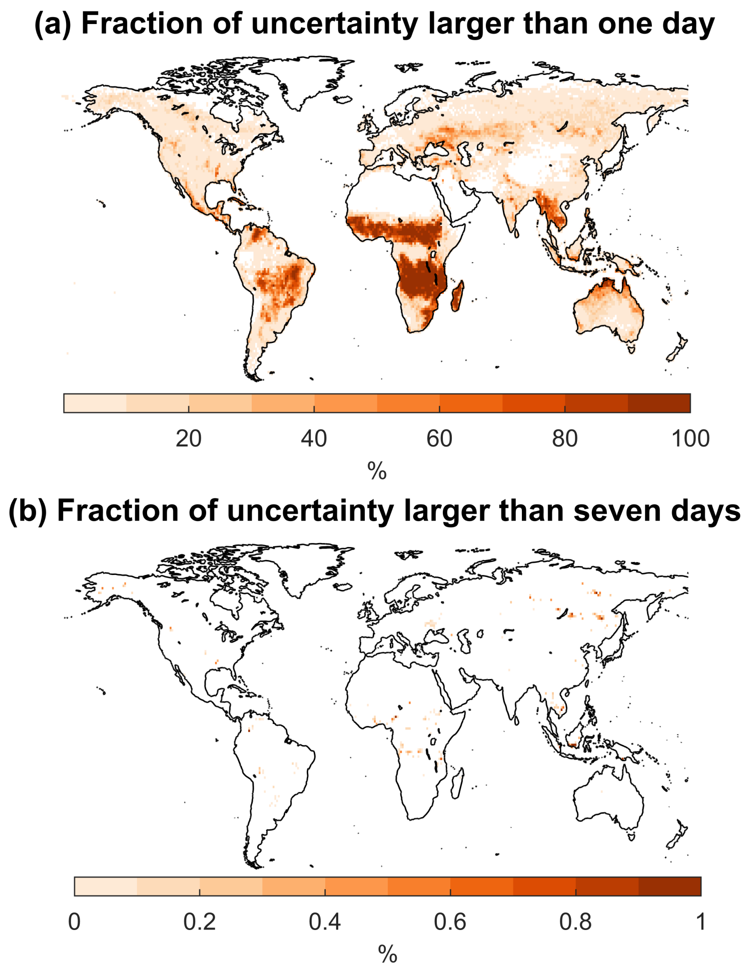

Figure S9. Uncertainty in burned date during fire season of 2002-2015. Fraction of days with burned date uncertainty larger than one (a) and seven (b) days out of the total number of days during the 2002-2015 fire season.

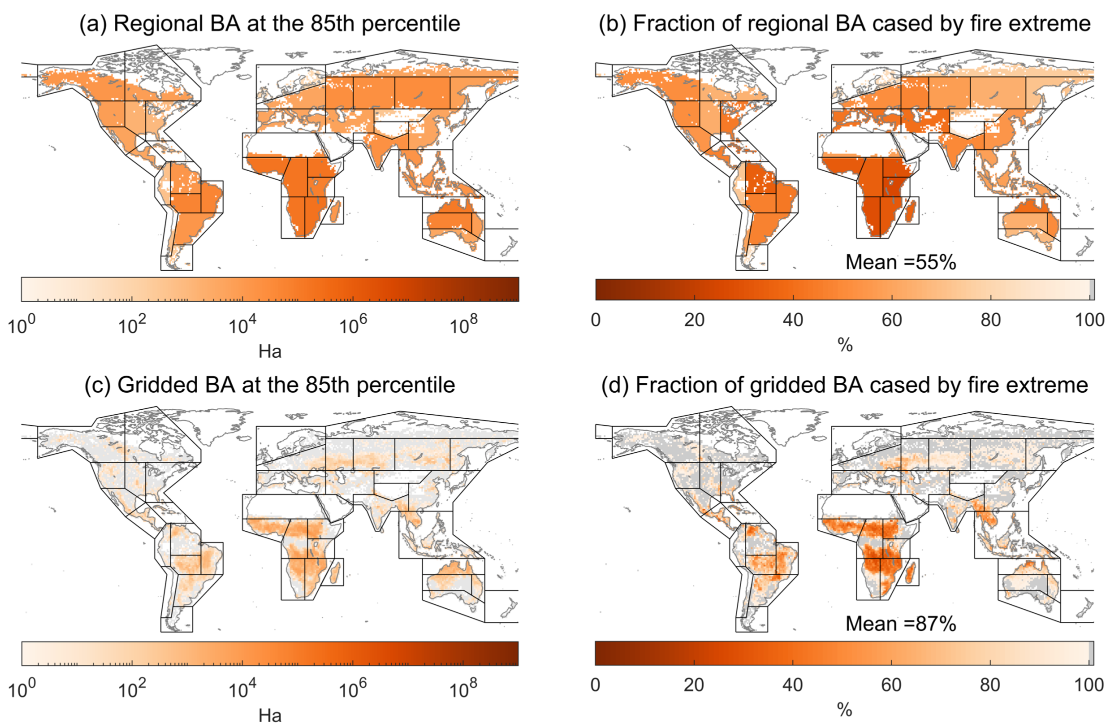

Figure S10. Fraction of burned area caused by extreme fire out of the total burned area during 2002-2015 fire season. (a) The regional burned area (BA) at the 85th percentile (regional values are derived from the sum of grid cells within each region; see Methods). A grey area means that BA at the 85th percentile is zero. (b) Fraction of regional burned area caused by extreme fire out of the total burned area during the 2002-2015 fire season over each region. Regional extreme fire is defined as weekly regional burned areas above the 85th percentile (see Methods). A fraction of 100% (grey) indicates that all burned areas in these locations are completely associated with the selected extremes. (c, d) Similar to panel a and panel b, respectively, but for the burned area at each grid cell. Gridded extreme fire is defined based on the same 85th-based methodology as regional extreme fire. The numbers on the bottom in panels b,d indicate the regional average across regions (b) and the spatially weighted average of the fractions across grid cells (d). Polygons show IPCC regions.

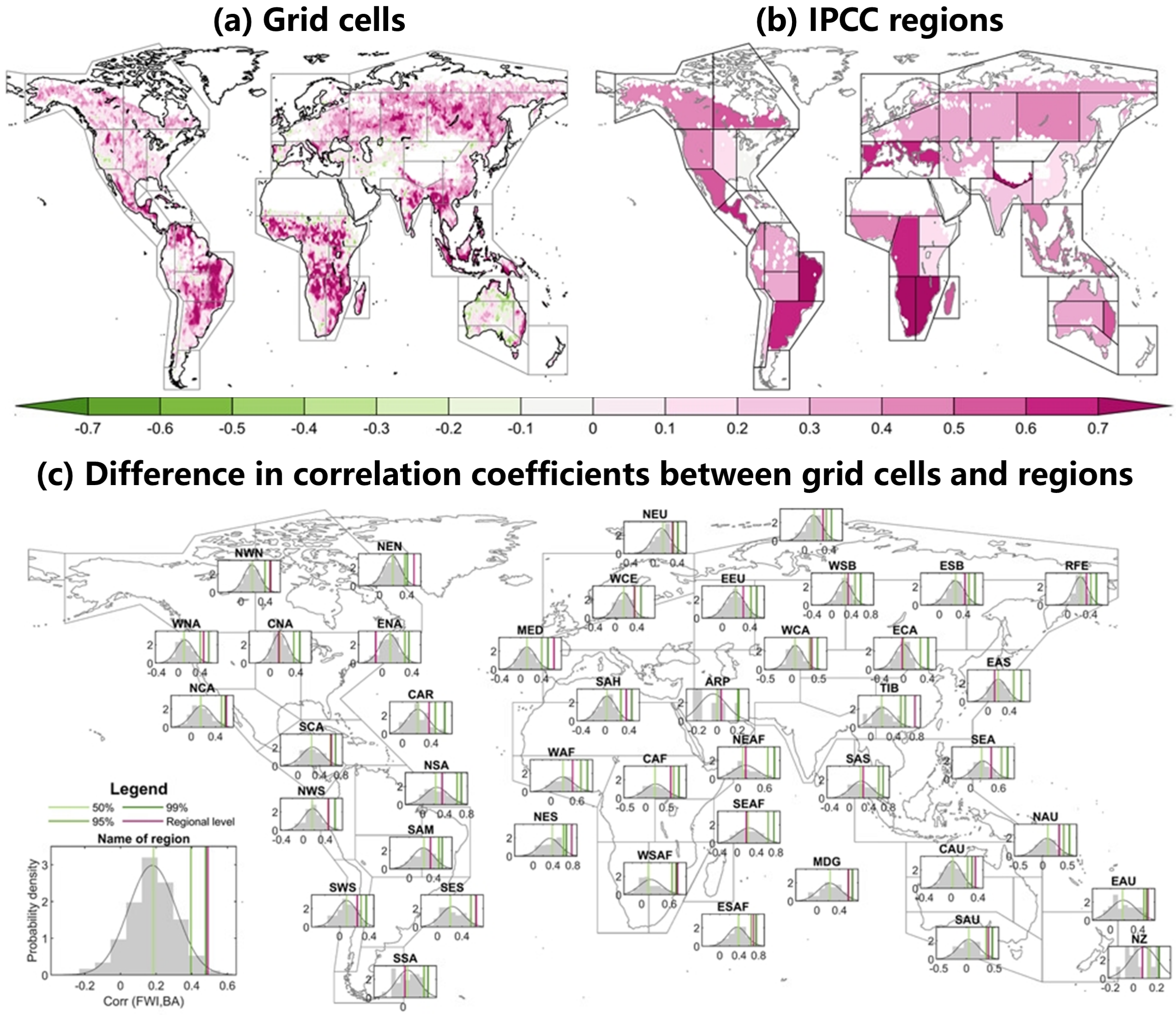

Figure S11. **The correlation between weekly Fire Weather Index (FWI) and burned area (BA) during the 2002-2015 fire season**. (a, b) The Spearman correlation between FWI and BA at the grid cells (a) and the regions (b). (c) The difference in correlation coefficients between grid cells and regions. The histogram with curve represents the probability density of the correlation coefficients for all grid cells over each IPCC region. The green lines from left to right indicate the 50th, 95th, and 99th of the correlation coefficient distribution across all grid cells over each IPCC region, respectively. The red line is the correlation coefficient between regional FWI and BA. Polygons show IPCC regions.

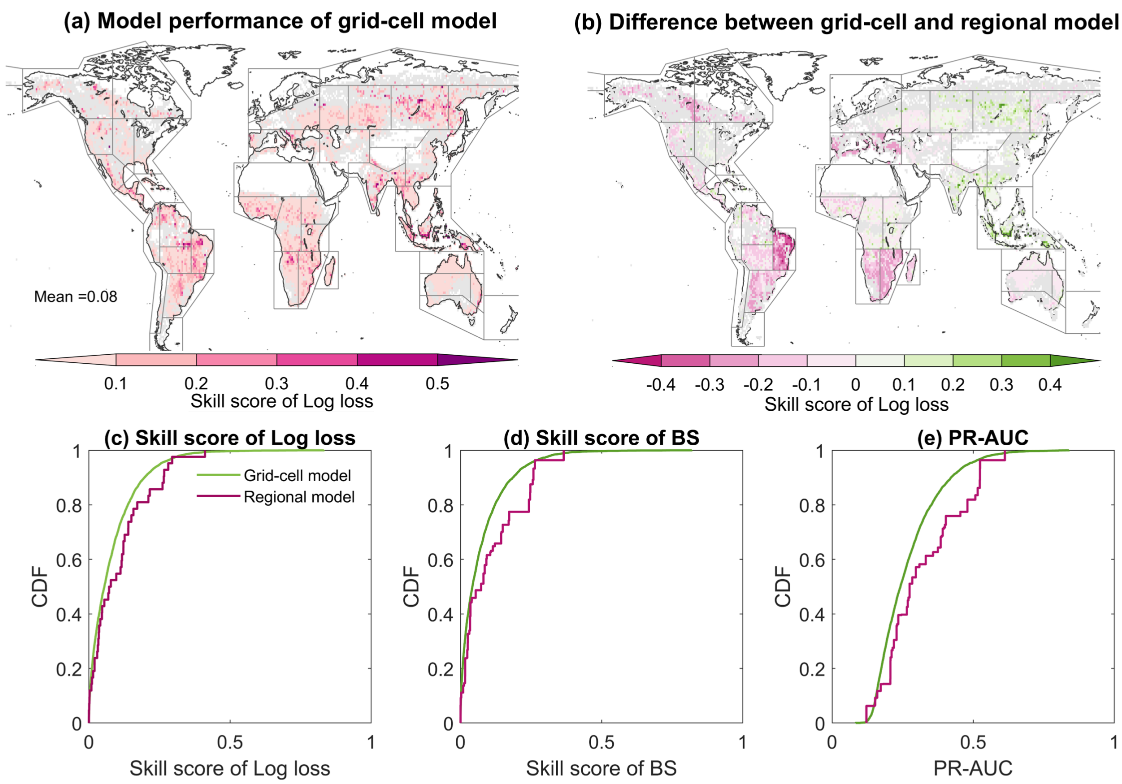

Figure S12. Performance of the grid-cell logistic regression models that predict the probability of weekly fire extremes based on observed Fire Weather Index (FWI). (a) The skill score of Log loss from the grid-cell model over grid cells while grey grid cells indicate locations, where we did not fit grid-cell because the 85th percentile of the BA is zero there (see Figure S10c). white areas indicate regions with no burned areas from 2001 to 2015. The numbers on the bottom left are the spatially weighted average of the scores from the grid-cell model. (b) Difference between the skill score of the gird-cell and regional model from Figure 1a over each IPCC region (values below zero indicate better skill of the regional model). Grey polygons in panel a-b show IPCC regions. (c) The cumulative distribution function (CDF) of the skill score across grids from the grid-cell model (green line) and across regions from the regional model (magenta line) in Figure 1a. (d-e) Similar to panel c but for skill score of Brier score (BS, d) and an area under the Precision-Recall curve (PR-AUC, e)

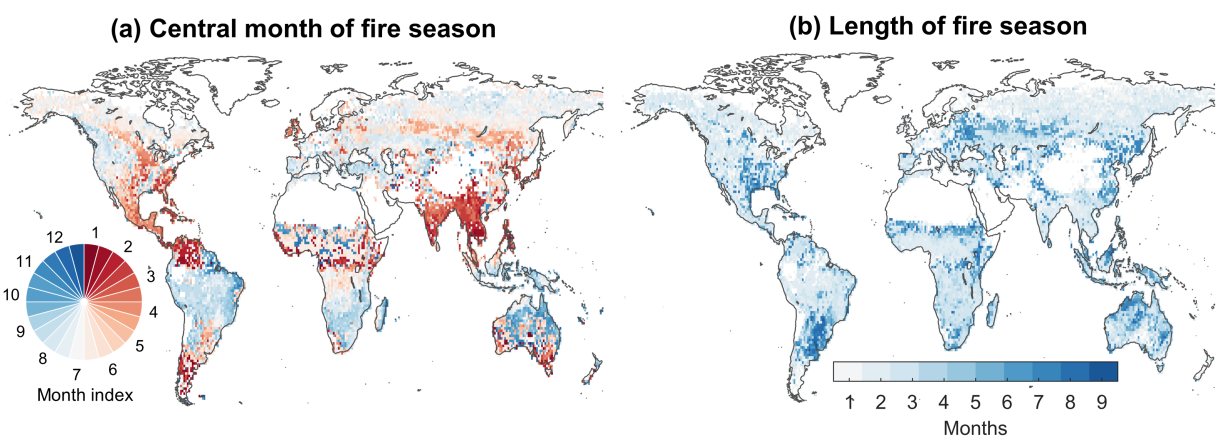

Figure S13. **Fire season at grid cells.** (a) Central month of fire season and (b) fire season length at individual grid cells. The fire season is defined based on the same procedure as Figure S8 but for each grid cell. The circular legend in the lower left of the panel a uses a 0.5 interval scale from 1 to 12.5 to consider the non-integer central months index.